Mechanism of micro-waviness induced KH_2PO_4 crystal laser damage and the corresponding vibration source*

Li Ming-Quan(李明全)[a], Chen Ming-Jun(陈明君)[a]†, An chen-Hui(安晨辉)[b], Zhou Lian(周 炼)[b], Cheng Jian(程 健)[a], Xiao Yong(肖 勇)[a], and Jiang Wei(姜 伟)[a]

[a] *Center for Precision Engineering, Harbin Institute of Technology, Harbin* 150001, *China*
[b] *Chengdu Fine Optical Engineering Research Center, Chengdu* 610041, *China*

(Received 14 March 2011; revised manuscript received 6 December 2011)

The low laser induced damage threshold of the KH_2PO_4 crystal seriously restricts the output power of inertial confinement fusion. The micro-waviness on the KH_2PO_4 surface processed by single point diamond turning has a significant influence on the damage threshold. In this paper, the influence of micro-waviness on the damage threshold of the KH_2PO_4 crystal and the chief sources introducing the micro-waviness are analysed based on the combination of the Fourier modal theory and the power spectrum density method. Research results indicate that among the sub-wavinesses with different characteristic spatial frequencies there exists the most dangerous frequency which greatly reduces the damage threshold, although it may not occupy the largest proportion in the original surface. The experimental damage threshold is basically consistent with the theoretical calculation. For the processing parameters used, the leading frequency of micro-waviness which causes the damage threshold to decrease is between 350^{-1} μm^{-1} and 30^{-1} μm^{-1}, especially between 90^{-1} μm^{-1} and 200^{-1} μm^{-1}. Based on the classification study of the time frequencies of micro-waviness, we find that the axial vibration of the spindle is the chief source introducing the micro-waviness, nearly all the leading frequencies are related to the practical spindle frequency (about 6.68 Hz, 400 r/min) and a special middle frequency (between 1.029 Hz and 1.143 Hz).

Keywords: laser induced damage threshold, micro-waviness, Fourier modal theory, power spectrum density

PACS: 03.50.Kk, 42.62.Eh, 42.70.Mp, 42.79.Nv **DOI:** 10.1088/1674-1056/21/5/050301

1. Introduction

Inertial confinement fusion (ICF) is one of the most effective ways to solve the problem of energy deficiency.[1] KH_2PO_4 (KDP) crystals are popularly used in the terminal optical system of ICF for frequency multiplication and Pockels cells.[2] However, the current low laser induced damage threshold (LIDT) of the KDP crystal (about 12 J/cm^2, 1064 μm, 3–5 ns) has become a bottleneck, which restricts the application and development of ICF.[3] Nowadays, most of studies on the LIDT of the KDP crystal focus on the factors inside the KDP crystal. Carr *et al.*[4] studied the influence of factors like stationary-state and transient-state deficiencies inside the crystal on the LIDT of the KDP crystal. Paul *et al.*[5] discussed the relationship between the inner impurity and the LIDT of the KDP crystal. Wang *et al.*[6] discussed the reasons for the light induced damage of the KDP crystal based on the mechanism of emerging and stabilizing of electron–hole, multi-photon ionization, and collision ionization inside the crystals. However, the machined surface quality (waviness, roughness, subsurface damage, relief stress induced by processing, etc) of the KDP crystal also has important effects on its LIDT.

Because KDP is soft and brittle and is extremely easy to deliquesce, single point diamond turning (SPDT) is the best method to process it.[7] However, after testing the machined surface morphology of KDP processed by the SPDT method, we find unreasonable mid-frequency waviness along the cutting path, which is called the micro-waviness. The micro-waviness will add periodic micro disturbance to the transmission wave front, and sometimes the structure of the micro-waviness is similar to the gratings. The near-field modulation of the micro-waviness can lead to a nonlinear increase of the laser intensity[8] and consequently lower the LIDT.[9] Therefore, studying the effects of the micro-waviness on the KDP crystal

*Project supported by the National Natural Science Foundation of China (Grant No. 50875066).
†Corresponding author. E-mail: chenmj@hit.edu.cn
© 2012 Chinese Physical Society and IOP Publishing Ltd

LIDT and finding the chief sources which introduce the waviness not only can provide the theoretical basis for increasing the LIDT, but also can guide the course of KDP processing and the improvement of machine structure. In this paper, we analyse quantitatively the influence of the micro-waviness on the LIDT of the KDP crystal, and study the chief sources that introduce these micro-wavinesses from the perspective of machine parts based on the combination of the Fourier modal theory and the power spectrum density (PSD) method.

2. Physical model of micro-waviness and Fourier model theory

The size of the micro-waviness period and amplitude are in the nm scale. The traditional scalar diffraction theory is not suitable for such small dimensions. Therefore, we use the Fourier model theory based on the rigorous electromagnetic field theory to solve the effects of diffraction of micro-waviness.[10−12] The ideal pattern of the micro-waviness is approximated by a sine wave as shown in Fig. 1, and the sine wave is approximated by a multilayer structure. The micro-waviness cross section is in the x–z plane with the y axis parallel to the micro-waviness line, the z axis is perpendicular to the substrate layer plane. The first and the (P_0+1)-th layers are the incident and the emergent air layers, respectively. The second to the (P_0-1)-th layers are the micro-waviness layers , and the P_0-th layer is the substrate layer.

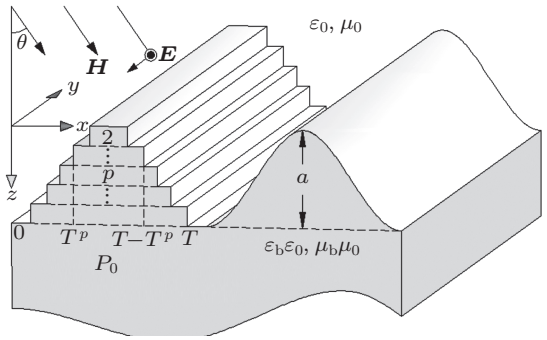


Fig. 1. Physical model of micro-waviness (two periods).

In each layer, the electromagnetic field satisfies the Maxwell equations

$$\boldsymbol{\nabla}\times\boldsymbol{E}=-\partial\boldsymbol{B}/\partial t,\quad \boldsymbol{\nabla}\times\boldsymbol{H}=\partial\boldsymbol{D}/\partial t, \tag{1}$$

where $\boldsymbol{E}$ is the electric field, $\boldsymbol{H}$ is the magnetic field, $\boldsymbol{D}=\varepsilon\boldsymbol{E}$, $\boldsymbol{B}=\mu\boldsymbol{H}$, $\varepsilon=\varepsilon_0\varepsilon_\mathrm{b}$, and $\mu=\mu_0\mu_\mathrm{b}$, ε_0 is the vacuum permittivity, ε_b is the relative permittivity of the material, μ_0 is the vacuum permeability, and μ_b is the relative permeability of the material. In the p-th layer, ε, μ, $\boldsymbol{E}$, and $\boldsymbol{H}$ are periodic with a period of T (with the amplitude of a). They can be written in the Fourier modal form as

$$[\varepsilon,\mu]^p=[\varepsilon_n,\mu_n]^p\exp\left(\mathrm{i}2\pi nx/T\right), \tag{2}$$

$$\begin{aligned}[\boldsymbol{E},\sigma\boldsymbol{H}]^p=&\exp\left(\mathrm{i}k_0\alpha_m x\right)\\&\times[e_{xm}\ e_{ym}\ e_{zm},-h_{xm}\ h_{ym}\ h_{zm}]^p\\&\times\exp\left[\mathrm{i}k_0\gamma^p\left(z-z^p\right)\right],\end{aligned} \tag{3}$$

where z^p is the upper interface coordinate of layer p; $\alpha_m=\alpha_0+\lambda m/T$, $m=0,\pm1,\pm2,\ldots,\pm M\ldots$; γ^p is related to the z axis component of wave number in layer p; k_0 is the vaccum wave number; and $\alpha_0=\sin\theta$, with θ being the incident angle.[13]

Concerning the discontinuation of two different media of the micro-waviness layers in the x axis (T^p is the interface coordinate), we use the Fourier inverse regulation factorization theory.[14,15] Substituting Eqs. (2) and (3) into Eq. (1), we obtain the eigenequation of transverse electric (TE) wave as

$$\begin{cases}\boldsymbol{A}\boldsymbol{e}_y=\boldsymbol{e}_y\boldsymbol{\gamma}^2,\\ \boldsymbol{h}_x=\bar{\boldsymbol{\mu}}\boldsymbol{e}_y\boldsymbol{\gamma},\quad \boldsymbol{h}_z=\boldsymbol{\mu}^{-1}\boldsymbol{\alpha}\boldsymbol{e}_y,\end{cases} \tag{4}$$

where $\boldsymbol{A}=\bar{\boldsymbol{\mu}}^{-1}\left(\boldsymbol{\varepsilon}-\boldsymbol{\alpha}\boldsymbol{\mu}^{-1}\boldsymbol{\alpha}\right)$; $\boldsymbol{\varepsilon}$, $\bar{\boldsymbol{\varepsilon}}$, $\boldsymbol{\mu}$, and $\bar{\boldsymbol{\mu}}$ are $(2M+1)$ square matrices obtained according to the inverse regulation theory; $\boldsymbol{e}_y$, $\boldsymbol{h}_x$, and $\boldsymbol{h}_z$ are $(2M+1)\times1$ matrices (matrix element of $\boldsymbol{e}_y$ is e_{ym}) for evaluation by the eigenequation; and $\boldsymbol{\alpha}$ is a $(2M+1)$ diagonal matrix with the matrix element being α_m.

From Eq. (4), we are able to obtain the eigenvector matrix $\boldsymbol{W}_{ey}$ consisting of $(2M+1)$ eigenvectors, and the eigenvalue matrices $\boldsymbol{\Gamma}_+$ and $\boldsymbol{\Gamma}_-$ composed of $(2M+1)$ positive eigenvalues and $(2M+1)$ negative eigenvalues, respectively, where $\boldsymbol{\Gamma}_+$ represents the upgoing wave, and $\boldsymbol{\Gamma}_-$ represents the downlink wave.

The general solution of the modal field is a linear superposition of the eigenmode fields. In layer p, the y component of electric-field intensity and the x component of magnetic-field intensity can be written as

$$\begin{cases} \boldsymbol{E}_y^p = \exp\left(\mathrm{i}k_0\alpha x\right)\boldsymbol{W}_{ey}^p\left\{\exp\left[\mathrm{i}k_0\boldsymbol{\Gamma}_+^p\left(z-z^p\right)\right]\boldsymbol{u}^p + \exp\left[\mathrm{i}k_0\boldsymbol{\Gamma}_-^p\left(z-z^p\right)\right]\ \boldsymbol{d}^p\right\}, \\ \sigma\boldsymbol{H}_x^p = \exp\left(\mathrm{i}k_0\alpha x\right)\left(-\boldsymbol{W}_{\mathrm{h}x}^p\right)\left\{\exp\left[\mathrm{i}k_0\boldsymbol{\Gamma}_+^p\left(z-z^p\right)\right]\boldsymbol{u}^p - \exp\left[\mathrm{i}k_0\boldsymbol{\Gamma}_-^p\left(z-z^p\right)\right]\boldsymbol{d}^p\right\}, \end{cases} \tag{5}$$

where σ is the conductivity of the material, $\boldsymbol{u}^p$ and $\boldsymbol{d}^p$ are two column vectors composed of eigenmode field amplitude coefficients of up-going and downlink waves, respectively, which can be solved by an algorithm of recursion reflection–transmission coefficient matrix (RTCM).[16–18]

The light intensity can be obtained using the following equation:

$$I = \frac{1}{2}\left|\mathrm{Re}(\boldsymbol{E}\times\boldsymbol{H}^*)\right|. \tag{6}$$

Assume that the incident light intensity through the KDP crystal is I, the relative laser induced damage threshold (T_{R}) is defined as

$$T_{\mathrm{R}} = I/I_{\max}, \tag{7}$$

where $I_{\max}$ is the maximum light intensity inside the crystal after the micro-waviness modulation. The T_{R} represents the degree to which the LIDT decreases, which means that the smaller the T_{R} is, the larger the LIDT decreases.

3. Experiments of KDP SPDT machining and LIDT testing

We firstly divide the sample surface into 18 areas and cut each area using the SPDT method with different processing parameters. The specific processing parameters are shown in Table 1. The topography of each area is then detected using an atomic force microscope (AFM) and a white light interferometer (WLI). Take area 1 of group B for example, the results are shown in Figs. 2(a) and 2(b).

Table 1. Cutting conditions for KDP samples..

Conditions	Group No.		
	A	B	C
Spindle speed /r·min^{-1}	400	400	400
Cutting speed/m·min^{-1}	792	792	792
Depth of cut/μm	10	15	20
Feed rate/μm·s^{-1}	7, 47, 73, 100, 133, 200	7, 47, 73, 100, 133, 200	7, 47, 73, 100, 133, 200
Tool rank angle/(°)	–45	–45	–45
Tool nose radius/mm	5	5	5

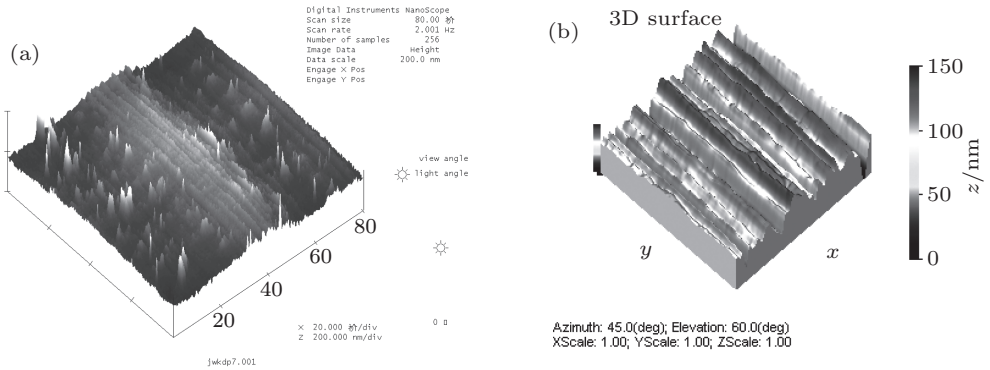


Fig. 2. Three-dimensional (3D) topographies of KDP surface processed by SPDT method (area 1 of group B) obtained by (a) AFM and (b) WLI.

From Fig. 2, we can obviously see the periodic tool marks, which show that the sine wave model of micro-waviness is feasible to a certain extent. We carry out the laser damage experiment for each KDP sample using a tri-band Nd: YAG Q-laser of single longitudinal mode, which is able to stably and effectively output

the TEM_{00} mode laser at the wavelength of 1064 nm. The laser path is shown in Fig. 3. The testing work takes the 1-on-1 mode. There are 20 testing areas on each sample, and the testing areas are separated by 3 mm or more to avoid the interfering. The experimental parameters used are given in Table 2.

We take the mean of the lowest two energy densities at which the KDP is damaged and the largest two energy densities at which the KDP is not damaged as the LIDT of the KDP crystal, and consider their standard deviation as the error. The experimental LIDTs for different testing areas of the KDP sample are given in Table 3.

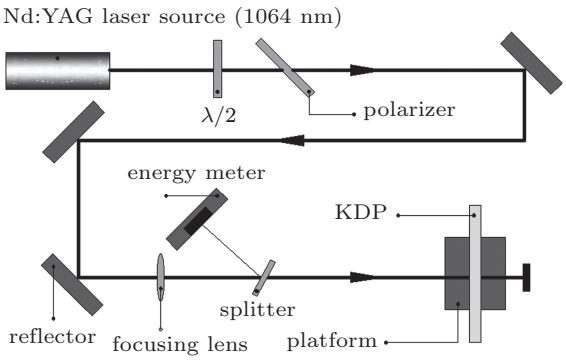


Fig. 3. LIDT experiment setup.

Table 2. Parameters used in the LIDT experiment.

Parameters of the laser beam path system					Environmental parameters		
Pulse width/ns	Optical divide ratio	Wavelength λ/nm	Focal rea A/mm^2	Incident angle	Vacuum state	Temperature	Moisture
4.5	1:25	1064	0.3784	0°	atmosphere	20–23°	72%

Table 3. Experimental data of LIDT of KDP crystal (J/cm^2).

Testing area	Group No.		
	A	B	C
1	12.78±0.95	13.40±1.00	12.26±0.71
2	14.63±0.60	12.45±1.01	8.63±0.49
3	14.65±0.44	11.97±0.47	8.50±0.37
4	15.64±0.93	12.18±0.41	8.01±0.62
5	15.10±0.40	11.46±0.51	9.44±0.64
6	16.33±0.81	12.08±0.56	9.02±0.69

4. Results and discussion

4.1. Obtaining frequency and amplitude information of micro-waviness

Firstly, we analyse the frequency and the amplitude information of the micro-waviness on the KDP surface. The relationship between the PSD and the amplitude of frequency f_m is[19,21]

$$a(f_m) = 2\sqrt{2 \times \mathrm{PSD}(f_m)\Delta f}, \tag{8}$$

where Δf is the sampling frequency, $\Delta f = f_{m+1} - f_m$.

For the surface shown in Fig. 2, the one-dimensional average PSD curve of surface profile along the x axis is shown in Fig. 4. From Fig. 4, we can see that the topography of the KDP surface consists of lots of frequency components, and several sub-waviness components with the characteristic periods marked in Fig. 4 account for the greatest proportion. The micro-waviness with the period of 437.5 μm occupies the largest proportion of the original surface, that with the period of 291.67 μm occupies the

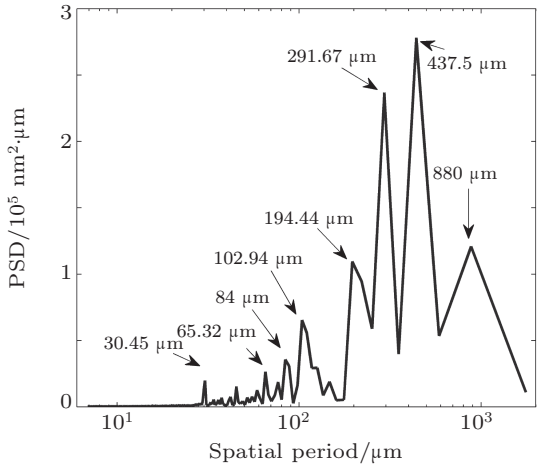


Fig. 4. PSD curve of area 1 of group B KDP sample.

second largest proportion, and those with the periods of 880 μm, 194.44 μm, 102.94 μm, 84 μm, 65.32 μm, and 30.45 μm are also significant. We should specially notice the micro-waviness of spatial period of 30.45 μm, which is nearly consistent with the feed of 30 μm. It is in fact the tool marks on the KDP surface. These sub-waviness components are all potential factors that cause the LIDT to decrease. The sub-waviness topography with the characteristic frequency can be obtained by the multi-scale decomposition of the original surface using the two-dimensional continuous wavelet transform (Wavelet: Mexican2d).[22,23] Figure 5 shows four examples of the 3D topography of the micro-wavinesses with the characteristic frequencies. Each frequency is related to a certain processing factor. We can find these factors and control them effectively.

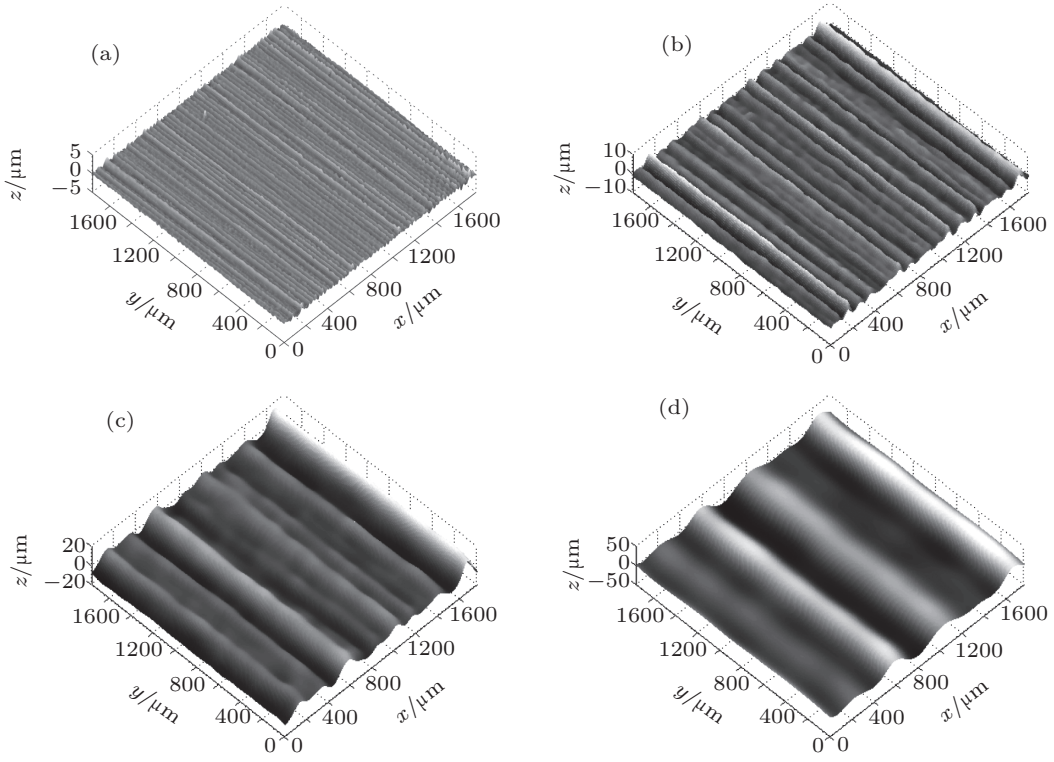


Fig. 5. 3D topographies of micro-wavinesses with the characteristic periods of (a) 30.45 μm, (b) 84 μm, (c) 194.44 μm, and (d) 437.5 μm on the original KDP surface.

4.2. Influence of micro-waviness on LIDT

With the Fourier model method, we create a simulation code to calculate the light intensity distribution inside the KDP crystal. Having found the characteristic frequencies on the KDP surface, we can obtain the amplitude information using Eq. (8). Then we are able to use our code to analyse the influence of micro-waviness on the LIDT of the KDP crystal. We assume that the incident wave is in the TE mode plane with a normalized amplitude and incident angle $\theta = 0°$. Figure 6 shows the relative thresholds with different spatial periods of micro-waviness on the surface of area 6 of group A. From Fig. 6 and by comparing it with Fig. 4, we can see that different micro-wavinesses have different influences on the LIDT of KDP. Although the micro-waviness of period 437.5 μm occupies the largest proportion on the original surface, it does not greatly reduce the LIDT. The micro-waviness of period 102.94 μm leads to a sharp reduction of 5% with respect to the LIDT of KDP, but it only occupies the fourth largest proportion on the KDP surface.

Figure 7 shows the distributions of light intensity modulated by the micro-wavinesses with the spatial periods of 65.32 μm, 102.94 μm, and 437.5 μm inside the KDP crystal. From Fig.7, we can clearly see that the micro-waviness of period 102.94 μm has a larger modulation degree than the other frequency components at the same laser propagation distance. The larger peak intensity lowers the LIDT.

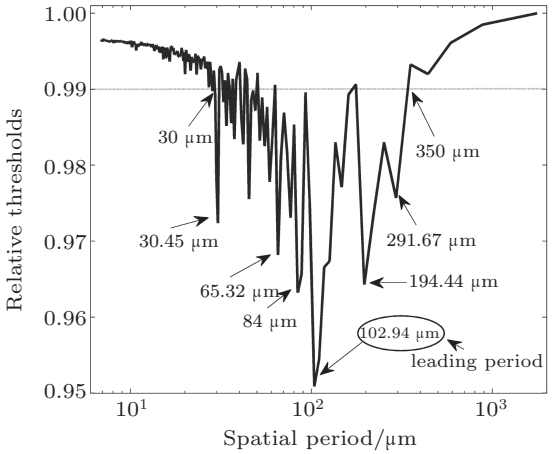


Fig. 6. Relative thresholds on the surface of area 6 of group A.

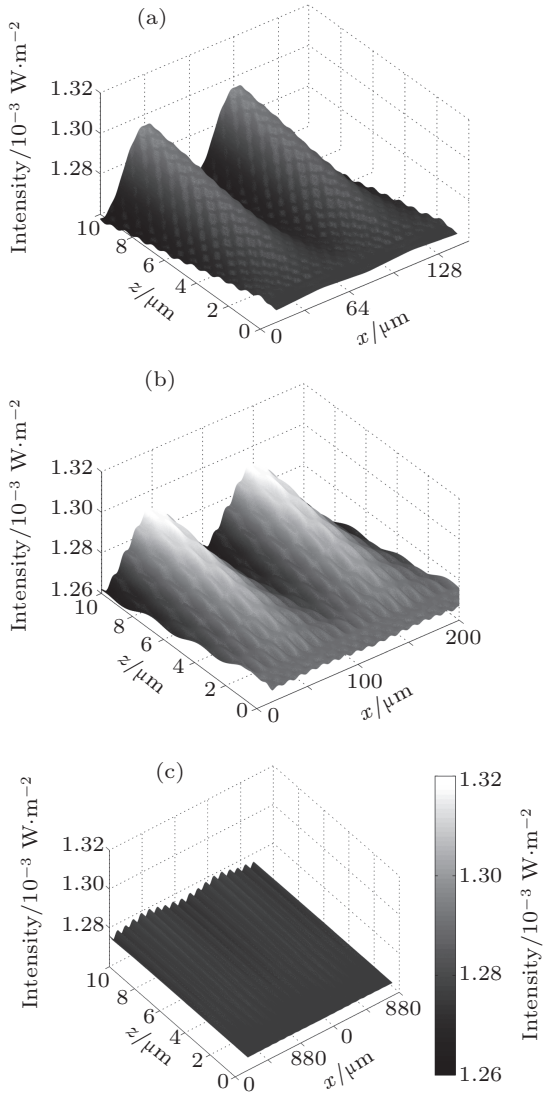


Fig. 7. Light intensity distributions inside the KDP sample with the spatial periods of (a) 65.32 μm, (b) 102.94 μm, and (c) 437.5 μm.

We consider the lowest value of the relative threshold curve as the relative threshold of the corresponding area, and consider the corresponding frequency of micro-waviness as the leading frequency. The relative threshold of this area is 95.09%, the leading frequency corresponds to the period of 102.94 μm. Table 4 provides the relative thresholds of all the 18 machined areas, and Table 5 gives the corresponding leading spacial periods. If we consider 0.99 as the minimum limit of relative threshold, we find that the processing factors that bring in the periods between 30 μm and 350 μm should be controlled effectively, and especially the ones between 90 μm and 200 μm.

Table 4. Relative thresholds of all areas (in percentage).

Area No.	Group No.		
	A	B	C
1	88.69	97.84	98.2
2	94.09	95.96	95.7
3	94.42	94.01	94.22
4	93.76	94.77	92.31
5	94.72	94.00	93.32
6	95.09	94.91	93.93

Table 5. Leading spacial periods of all areas (in μm).

Area No.	Group No.		
	A	B	C
1	134.62	194.44	116.67
2	83.33	92.11	116.67
3	145.83	92.11	145.83
4	145.83	116.67	145.83
5	250.00	102.94	194.44
6	102.94	194.44	154.40

Figure 8 shows the comparison between the theoretical relative thresholds provided in Table 4 and the experimental LIDTs provided in Table 3. From Fig. 8(b), we can see that the changing regulations of the theoretical value and the experimental data with different feeds are completely consistent when the depth of cut is 15 μm. From Figs. 8(a) and 8(c), we can see that the fitting curve of experimental data is in accordance with the theoretical data, although the changing trend between two neighboring points does not strictly accord with the experimental error extent, comparing the curves generally shows the same changing trend. As a whole, the experimental LIDTs and the theoretical relative thresholds accord very well with each other. From the discussion above, we can conclude that the micro-waviness model established by us and the combination of the Fourier model method and the PSD method are feasible for

analysing the influence of micro-waviness which exists on the KDP surface processed by the SPDT.

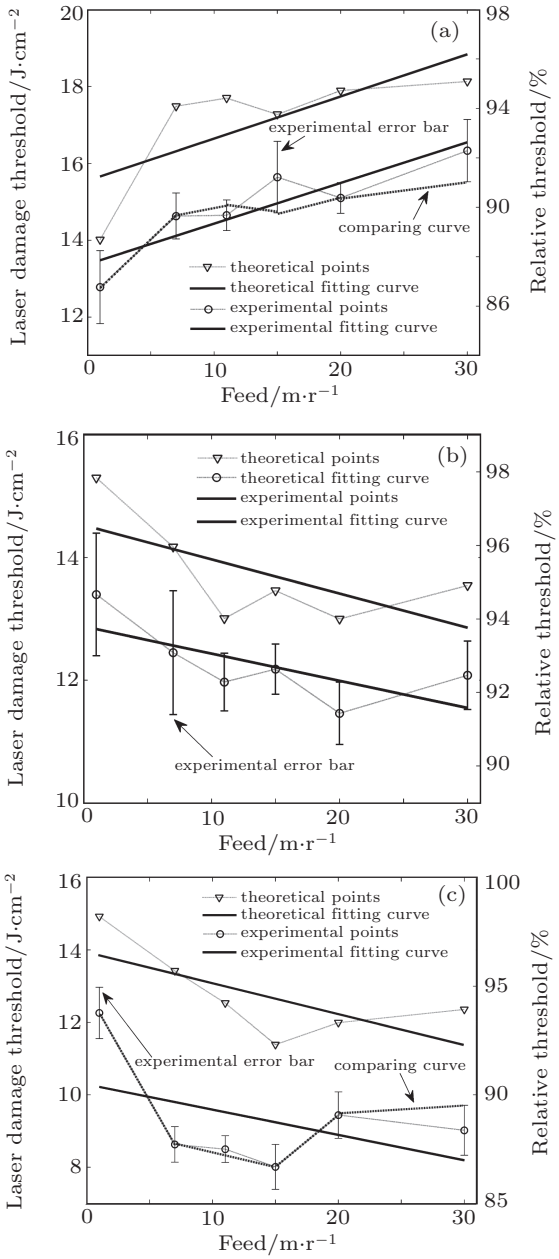


Fig. 8. Comparing theoretical relative thresholds with the experimental LIDTs for (a) a_p=10 μm; (b) a_p=15 μm; (c) a_p=20 μm (a_p is the cutting depth).

4.3. Analysis of the vibration sources which introduce micro-waviness

From the discussion above, we can see that the micro-wavinesses, especially the ones with the leading frequencies, induced by the SPDT method have important effects on the LIDT of the KDP crystal. Therefore, finding the processing factors corresponding to these micro-wavinesses is critical for reducing or eliminating the influence of micro-waviness on the LIDT of the KDP crystal.

The SPDT allows the direct obtainment of sub micrometric form accuracy with nanometric roughness without complementary operations such as lapping or polishing,[24] so it is widely used in processing high-quality optical elements. The machine adopts a vertical architecture, the spindle installed on aerostatic bearings is mounted axially in the z direction. The slides are fixed on a massive granite block, which itself is located on four self-leveling pneumatic isolators. A large disk is fixed on the bottom of the principle axis, and the diamond tool is fixed at the edge of the big disk. Because of the special structure of the SPDT machine, if the spindle is not strictly vertical to the surface of the workpiece, the slight vibration of the spindle will lead to several-fold vibration between the tool and the surface. Therefore, the spindle vibration may be the main cause of micro-waviness during the processing in the SPDT method. Of course, we cannot completely neglect the effects of other elements, such as the straightness of the slides, the anisotropy of the material, and the environmental vibration.[25,26] An *et al.*[27] established Euler's dynamic equations for the angular displacement calculation of gas spindles, and pointed out theoretically that a middle frequency which is a fraction of the spindle frequency (6.25 Hz, with their processing parameters) exists as a main factor inducing the micro-waviness on the KDP surface. With the SPDT machine specially built for processing the KDP crystal in Haerbin Institute of Technology, they tested the axial vibration of the spindle and found that the middle frequency was about 0.94 Hz (1.07 Hz in theory). When the spindle speed was 400 r/min, the experimental value of spindle frequency was 6.41 Hz, and the theoretical time frequency is 6.67 Hz, the error is caused mainly by the fluctuation of the spindle speed.

The relationship between the time frequency of micro-waviness and its spatial frequency is

$$f_{\mathrm{t}} = \frac{1}{60} f_{\mathrm{k}} v f, \tag{9}$$

where f_{k} is the spatial frequency in μm^{-1}; v is the spindle speed in r/min; and f is the feed in μm/r.

Using Eq. (9), we can obtain the time frequencies corresponding to the characteristic spatial frequencies in all the 18 machined areas. We classify these values based on the multiple relationship between them, the result is shown in Table 6. From Table 6, we can see that there are about four sources that induce

the micro-waviness on the KDP surface. The base frequency is about 6.48–6.86 Hz in group 1, which is nearly equal to the spindle frequency (6.67 Hz in theory). So, we know that the micro-wavinesses in group 1 are induced by the spindle frequency. These micro-wavinesses are related to the feeds, and their periods are the integer multiples of the tool marks on the KDP surface. The base frequency of group 2 is between 1.029 Hz and 1.143 Hz. The middle frequency mentioned above (1.0672 Hz in theory) is in this range. So, we know that all the micro-wavinesses in group 2 are related to the middle frequency. From the data in group 2, we are able to conclude that this middle frequency is truly the main factor that leads to the micro-waviness. The time frequencies of the leading frequencies provided in Table 5 are highlighted in Table 6. From the distribution of these marked data, we can see that the spindle vibration is the most important element that induces the micro-waviness on the KDP crystal. By improving the dynamic property of the spindle it could be possible to increase the LIDT of KDP. We do not know exactly the factors that cause the micro-wavinesses in groups 3 and 4, which will be investigated in depth in the future.

Table 6. Classification of time frequencies of micro-waviness.

Group No.	Time frequency/Hz	Base frequency/Hz
1	0.0686, **0.0343**,**0.6857**, 0.6857, 0.0343, 0.0686, **0.6857**, 0.6857, 0.0174, 0.0648, **1.2953**, **1.2953**, 1.3714	6.48–6.86
2	**0.5029**, 0.0498, 0.5143, **0.5333**, **0.5066**, **0.5029**, 0.5867, 0.2667, 0.0267, **0.0267**, 0.2743, 0.2514, 0.2933, 0.2857, **0.56**, 0.5714, **0.0571**, 0.1333, 0.1333, 0.1029, 0.1067, **1.0286**, 1.0667, 0.0114, 0.1143, 0.2286, 0.2273, 0.2272, 0.4571, **0.4571**, 0.0457, 0.4571, 0.4571, **0.5029**	1.029–1.143
3	0.08, **0.8**, 0.16, 0.8,**0.4**, 1.6, 0.8	1.6
4	0.019, 0.1943, 0.3772, 0.3810, 0.7619, 0.7619, **1.9429**, 1.9429,	1.9429

5. Conclusions

In this paper, we analyse the influence of micro-waviness on the LIDT of the KDP crystal based on the Fourier model method and the PSD method. In addition, we also briefly discuss the main sources that introduce the micro-waviness by studying the time frequencies of the micro-waviness. The following conclusions are obtained.

1) The surface topography of KDP processed by the SPDT method is composed of micro-wavinesses with different characteristic frequencies. The micro-waviness occupying the largest proportion of the KDP surface is not always the one that causes the greatest reduction in LIDT.

2) The micro-wavinesses with leading frequencies may appear repeatedly, and they are introduced by some intrinsic vibration elements of the machine.

3) If we consider 0.99 as the minimum limit of relative threshold, we find that the processing factors that bring in the frequencies between 350^{-1} μm^{-1} and 30^{-1} μm^{-1}, especially the ones between 200^{-1} μm^{-1} and 90^{-1} μm^{-1}, should be carefully controlled, because nearly all the leading frequencies are in this range.

4) The spindle axial vibration is a critical factor that introduces dangerous micro-wavinesses on the KDP surface. The practical spindle frequency (about 6.86 Hz, 400 r/min) and the special middle frequency (between 1.029 Hz and 1.143 Hz), introduce nearly all the dangerous micro-wavinesses on the KDP original surface.

References

[1] Moses E I and Meier W R 2008 *Fusion Engineering and Design* **83** 997

[2] Negres R A, Kucheyev S O, Mange P D, Bostedt C, Buuren T V, Nelson A J and Demos S J 2005 *Appl. Phys. Lett.* **86** 171107

[3] Tang Z Y, Yang J L, Wen S H, Wang G X, Guo Y Z, Yang H Q and Ma C 1999 *Acta Phys. Sin.* **48** 913 (in Chinese)

[4] Carr C W, Feit M D, Johnson M A and Rubenchik A M 2006 *Appl. Phys. Lett.* **89** 131901

[5] Paul D M, Negres R A, Radousky H B and Demos H G 2006 *Opt. Eng.* **45** 104205

[6] Wang K P, Fang C S, Zhang J X, Sun X, Wang S L, Gu Q T, Zhao X and Wang B 2006 *Journal of Crystal Growth* **287** 478

[7] Wang J H, Chen M J and Dong S 2005 *Opto-Electronic Engineering* **32** 67 (in Chinese)

[8] Chen M J, Jiang W and Li M Q 2010 *Chin. Phys.* B **19** 064203

[9] Chen M J, Li M Q, Jiang W and Xu Q 2010 *J. Appl. Phys.* **108** 043109
[10] Zhou C H and Li L F 2004 *J. Opt.* A **6** 43
[11] Yao X, Gao F H, Li J F, Zhang Y X, Wen S L and Guo Y K 2008 *Acta Phys. Sin.* **57** 4891 (in Chinese)
[12] Bai B F and Li L F 2006 *Opt. Commun.* **262** 140
[13] Bayanheshig, Qi X D and Tang Y G 2003 *Acta Phys. Sin.* **52** 1157 (in Chinese)
[14] Li L F 1993 *J. Opt. Soc. Am.* A **10** 2581
[15] Li L F 1998 *J. Opt. Soc. Am.* A **13** 1313
[16] Fu K X, Zhang D Y, Wang Z H, Zhang Q Z and Zhang J 1998 *Acta Phys. Sin.* **47** 1278 (in Chinese)
[17] Fu K X, Wang Z H, Zhang D Y, Zhang J and Zhang Q Z 1989 *Science in China Series* A: *Mathematics* **42** 636 (in Chinese)
[18] Ma J Y, Liu S J, Jin Y X, Xu C, Shao J D and Fan Z X 2008 *Opt. Commun.* **281** 3295
[19] Elson J M and Bennett J M 1995 *Appl. Opt.* **34** 201
[20] Lawson J K, Aikens D M, Englishjr R E and Wolfe C R 1996 *Proc. SPIE* **2775** 345
[21] Zhang R Z, Cai B W, Yang C L, Xu Q and Gu Y Y 2000 *Proc. SPIE* **4231** 295
[22] Zahouani H, Mezghani S, Vargiolu R and Dursapt M 2008 *Wear* **264** 480
[23] Jiang X Q, Zeng W H, Scott P, Ma J W and Blunt L 2008 *Wear* **264** 428
[24] Hatem K, Marc B and Philippe R 2005 *International Journal of Machine Tools & Manufacture* **45** 841
[25] Wang J H, Dong S, Wang H X, Chen M J, Zong W J and Zhang L J 2007 *Key Engineering Materials* **339** 78
[26] Chen M J, Pang Q L, Wang J H and Cheng K 2008 *International Journal of Machine Tools & Manufacture* **48** 905
[27] An C H, Wang J, Zhang F H, Xu Q and Chen D J 2010 *Nanotechnology and Precision Engineering* **8** 439